J Porous Mater (2016) 23:1537–1545
DOI 10.1007/s10934-016-0214-z

A facile strategy to fabricate carboxyl-rich carbon spheres with copper-based MOFs through coordination bond

Chunhua Ge[1] · Yan Du[1] · Rui Wang[1] · Lili Xue[1] · Zhongshuai Wu[2] · Tianzhu Xing[1] · Xiaochun Ji[1] · Lin Ma[1] · Xiangdong Zhang[1]

Published online: 18 June 2016

Abstract A new composite (CCSs/MOFs) of carboxyl-rich carbon spheres (CCSs) and copper-based metal–organic frameworks (MOFs) was for the first time prepared. The CCSs/MOFs composite was synthesized by the coordinated growth of high surface area and porous MOFs, $[Cu_3(BTC)_2(H_2O)]_n$ (HKUST-1), on the surface of the functionalized CCSs obtained through a one-step hydrothermal carbonization of glucose with acrylic acid at 180 °C for 24 h. The resulting composites showed a core/shell structure with a tunable diameter arranging from 0.6 to 3.0 μm, and possessed high specific surface area of 495 m^2/g and nanoporous structures derived from MOFs. Further, the catalytic oxidation of benzylic alcohol to benzaldehyde as its application was studied.

Keywords Carbon spheres · MOFs · Composites · Catalysis

1 Introduction

Metal–organic frameworks (MOFs) are constructed by linking metal-containing units with organic species, using strong bonds to create open crystalline yet well-defined porous frameworks, which are attracting considerable attentions as new inorganic–organic hybrid materials for a wide range of potential applications, including gas storage, separations, and catalysis, fuel cells, supercapacitors, and catalytic conversions [1–4].

One of the main advantages of the MOFs is their high surface area and exceptional porosity, which in particular exhibit great potential in the use of catalysts [5–7]. However, the low mechanical strength and block nature of the MOF products greatly prevent their application in these certain areas. To overcome this issue, great efforts have been made on designed synthesis of novel-type composites of MOFs with polymers or nanocarbons in recent years [8–10]. For instance, Schwab et al. [11] reported the in situ immobilisation of a MOF (HKUST-1) into a hydrophilized macroporous polyHIPE monolith, and revealed that the resulting HKUST-1@polyHIPE composites effectively combines the macroporosity of the polyHIPE with the microporosity of the crystalline MOF of HKUST-1, which is an attractive combination for applications where diffusion processes are limiting. Recently, Petit et al. [12, 13] reported the MOF-graphene oxide composites with high porosity and specific surface area can combine the uniqueness of graphene layers and MOF, exhibiting enhanced adsorption of ammonia due to the synergistic effect and surface interaction of oxygen-containing graphene and MOF.

In these sense, the MOF-based composites could significantly promote transport processes towards the microporous structure of the MOF, which is favorable for fast and efficient uptake and release kinetics in particular when diffusion-controlled processes are involved in catalytic systems [14–18].

In this study, we present the designed synthesis of a composite (CCSs/MOFs) of copper-based metal–organic frameworks (MOFs) of $[Cu_3(BTC)_2(H_2O)]_n$ (HKUST-1) deposited on hydrothermally synthesized carboxyl-rich

✉ Xiangdong Zhang
xd623@sina.com

[1] College of Chemistry, Liaoning University, Shenyang 110036, Liaoning, People's Republic of China

[2] Dalian National Laboratory for Clean Energy, Dalian Institute of Chemical Physics, Chinese Academy of Sciences, Dalian 116023, People's Republic of China

carbon spheres (CCSs) as a novel catalyst for efficient catalytic oxidation reaction of benzylic alcohol to benzaldehyde. The carboxyl-rich CCSs were synthesized using glucose and acrylic acid as carbon source by hydrothermal treatment. It is revealed that the acrylic acid derived carboxyl-rich groups of carbon spheres (CCSs) could significantly enhance the connection with the Cu ion in MOF, and benefit for the homogenous surface growth of HKUST-1 on the core of CCSs. Further, the resulting composite exhibited a core/shell structure with a tunable diameter, and possessed high specific surface area and nanoporous structures derived from MOFs. Importantly, these CCSs/MOFs composite hold great potential in the direct oxidation reaction of benzylic alcohol to the benzaldehyde, with an impressive yield.

2 Experimental procedure

2.1 Materials

The reagent of $Cu(NO_3)_2{\cdot}3H_2O$ was purchased from Aladdin. Benzyl alcohol, benzaldehyde, and nitrobenzene are purchased from Alfa Aesar. Other reagents are purchased from Sinopharm Chemical Reagent. The solvents used are chromatographic pure reagents, and the materials are used without any further pretreatment.

2.2 Synthesis

2.2.1 Synthesis of HTC

Typically, 32 g glucose was dispersed into redistilled water (144 mL) at room temperature. Then, 60 mL glucose solution was transported to a 100 mL Teflon-lined stainless steel autoclave and hydrothermally treated at 180 °C for 24 h. Subsequently, the obtained samples are washed three times with deionized water and ethanol, and dried overnight at 70 °C. Finally, the samples are activated in a muffle furnace under air atmosphere at 300 °C for 5 h.

2.2.2 Synthesis of CCSs

CCSs were synthesized by the method described previously [19]. Typically, 60 mL 1.12 mol/L glucose solution and a certain amount of acrylic acid ranging from 1.45 to 5.6 mL were mixed by sonication for 5 min. The synthesized CCSs are called CCS-1 (acrylic acid, 1.45 mL), CCS-2 (acrylic acid, 2.30 mL), CCS-3 (acrylic acid, 3.30 mL), and CCS-4 (acrylic acid, 5.60 mL). Then, the mixture was transported to a 100 mL Teflon-lined stainless steel autoclave and hydrothermally treated at 180 °C for 24 h. Subsequently, the obtained samples are washed three times with deionized water and ethanol, and dried overnight at 70 °C. Finally, the samples are activated in a muffle furnace under air atmosphere at 300 °C for 5 h.

2.2.3 Synthesis of HKUST-1

HKUST-1 was synthesized by the method described previously [20]. Specially, 2.1 g $Cu(NO_3)_2{\cdot}3H_2O$ and 1.0 g 1,3,5-benzenetricarboxylic acid (H_3BTC) were added into a mixed solvent comprising 17 mL dimethylformamide (DMF), 17 mL ethanol, and 17 mL H_2O by sonication. Then, the suspension was stirred and heated in a 100 mL round-bottom flask at 85 °C for 21 h in an oil bath, in which the stirring time was 20 h. After cooling down, the obtained sample was washed and immersed with dichloromethane for 3 days, and the dichloromethane was changed each 24 h. After that, the sample was dried at 170 °C for 28 h in a vacuum oven.

2.2.4 Synthesis of the CCS/HKUST-1 composites

Typically, 2.1 g $Cu(NO_3)_2{\cdot}3H_2O$ and 1.0 g H_3BTC were stirred and sonicated in the mixed solvent comprising 17 mL DMF, 17 mL ethanol, and 17 mL H_2O. After stirring for 30 min, the CCS-3 was added by sonication for 10 min. Then, the suspension was heated at 85 °C for 21 h in an oil bath, in which the stirring time was 20 h. After cooling down, the obtained sample was washed and immersed with dichloromethane for 3 days, and the dichloromethane was changed each 24 h. After that, the sample was dried at 170 °C for 28 h in a vacuum oven. The nomenclature of the resulting CCS/HKUST-1 composites is based on the added CCS content of 340, 510, 850 and 2589 mg, which was denoted as Composite-1, Composite-2, Composite-3, and Composite-4, respectively.

Hydrothermal carbon spheres (HTC) [14] were used to compare the influence of the carboxyl group of CCS-3. HTC-HKUST-1-A (510 mg HTC addition) and HTC-HKUST-1-B (850 mg HTC addition) were named.

2.3 Catalytic oxidation of benzylic alcohol

A 25 mL round-bottom flask was charged with 85 mg Na_2CO_3, 25 mg TEMPO (2,2,6,6-tetramethyl-1-piperidinyloxy as co-catalyst), and 150 mg Composite-1. Subsequently, 5 mL acetonitrile was added to this mixture followed by 95 μL benzyl alcohol. The mixture was then heated at 70 °C in an oil bath and stirred for 22 h. After that, the mixture was filtered, and the filtrate was transferred to a 10 mL flask and further diluted with acetonitrile. The yield from benzylic alcohol to the benzaldehyde was calculated using gas chromatography (GC) internal standard method with nitrobenzene as the internal standard.

2.4 Characterization

Fourier transform infrared spectroscopy (FT-IR) is conducted using PerkinElmer Spectrum One (USA) with a wave range of 4000–500 cm^{-1}. Powder X-ray diffraction (XRD) is recorded on a Bruker diffractometer using a Cu $K\alpha$ X-ray radiation with 45 kV voltage and 40 mA current. The samples are ground in a small agate mortar. The patterns are collected over 5°–50°. The microscopic features of the samples are obtained through scanning electron microscopy (SEM, JEOL-6701F and HITACHI SU8010) and transmission electron microscopy (TEM, JEOL JEM-1011, 100 kV and JEOL JEM-2100, 100 kV). The Cu content of Composites is analyzed by ICP-AES (PerkinElmer ICP-AES Optima8000) and EDS (HITACHI SU8010). The nitrogen sorption experiments are performed at 77 K using an automated gas sorption analyzer (AsiQ-C). The carbon dioxide sorption experiments are measured at 273 K using an automated gas sorption analyzer (AsiQ-C). Varian CP-3800 is employed to conduct GC measurement.

3 Results and discussion

Figure 1 presents the FT-IR spectra of the HTC and the CCSs with different acrylic acid contents. It can be seen that the HTC shows the vibrations of C=C and C=O are at 1603 and 1714 cm^{-1}, which represent the aromatic core of the HTC and the carboxyl group, respectively [19]. Note that the intensities of the stretching vibration of C=O at 1720 cm^{-1} and C–O at 1250 cm^{-1} gradually increase with increasing the content of acrylic acid, due to the increase of the number of the carboxyl groups. Furthermore, the increase in vibration of C=C at 1615 cm^{-1} indicates that

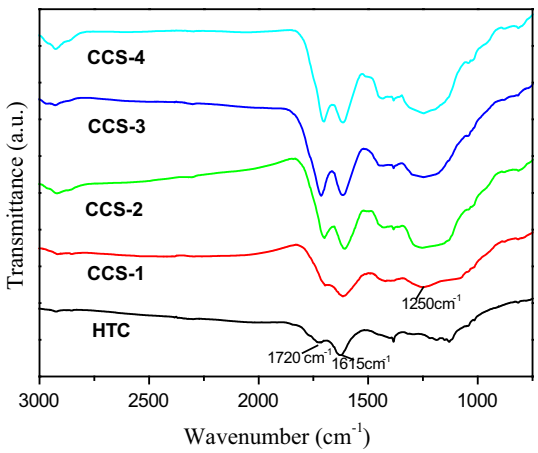

Fig. 1 FT-IR spectra of HTC and CCSs with different content of acrylic acid

the aromatic core of the carbon spheres became bigger. Additionally, the bending vibration of C–H at 1400 cm^{-1} increases, and the vibration around 2900 cm^{-1} are visible, indicative of the formation of the polyacrylic acid balls.

Figure 2 presents the SEM images of the HTC and the CCSs. It is shown that the carbon spheres of the HTC have an average diameter of 0.6 μm, and smooth surface morphology in Fig. 2a. This suggested the deposited amount of MOF on HTC is very limited due to the lack of the carboxyl groups on HTC. In contrast, the surface morphology of the CCSs becomes more and more roughness with increasing the content of the carboxyl groups in CCSs, originating from the addition of acrylic acid. Therefore, the diameter of the spherical carbon increases and their morphologies no longer become smooth, as shown in Fig. 2b, c. It is suggested that the acrylic acid increases the amount of carboxyl groups but that too much acrylic acid would occur self-polymerization to generate polyacrylic acid micro spheres under hydrothermal conditions (Fig. 2d). Therefore, CCS-3 is demonstrated as a better candidate than HTC to react with Cu^{2+}.

Figure 3 presents the FT-IR spectra of CCS-3, HKUST-1, and Composite-n. The HKUST-1 spectra show that the vibrations of carboxyl of BTC are at 1370 and 1445 cm^{-1} and at 1560 and 1610 cm^{-1} [21, 22]. The vibration of C=O is at 1610 cm^{-1} in HKUST-1, which corresponds to the carboxyl group on the BTC combining with Cu^{2+} (Fig. 3). The band at 1645 cm^{-1} in the Composite-1, Composite-2 and Composite-3 increases with increased CCS. However, because the amount of CCS was added too much in Composite-4, the band at 1645 cm^{-1} was influenced by the vibration of C=C at 1615 cm^{-1} in CCS, and combine with the band at 1610 cm^{-1} to form a new relatively wide peak. This phenomenon indicates that the interaction of the carboxyl groups on the CCSs with Cu^{2+} in HKUST-1 [10].

The phase structure of the CCSs, HKUST-1, HTC-HKUST-1, and Composite-n was further characterized by XRD patterns. As shown in Fig. 4, it can be seen that the CCS-3 only has a wide peak at about 25°. And the CCSs/MOFs composites (from Composite-1 to Composite-4) exhibited the similar diffraction peaks to the HKUST-1, indicative of the crystalline structure formation of HKUST-1 on the surface of CCSs. This result is consistent with that found in FT-IR (Fig. 3). The diffraction peaks of the HTC-HKUST-1 was high consistent of pure HKUST-1.

The morphology of the CCSs/MOFs composites and HTC-HKUST-1 was characterized by SEM and TEM images. As shown in Fig. 5a, the HKUST-1 blocks are well distributed when the CCSs content is low. This indicates that the CCSs are wrapped by the HKUST-1, and the conversion of CCSs is well. With increased CCSs content, the size of the CCSs/HKUST-1 composite become smaller

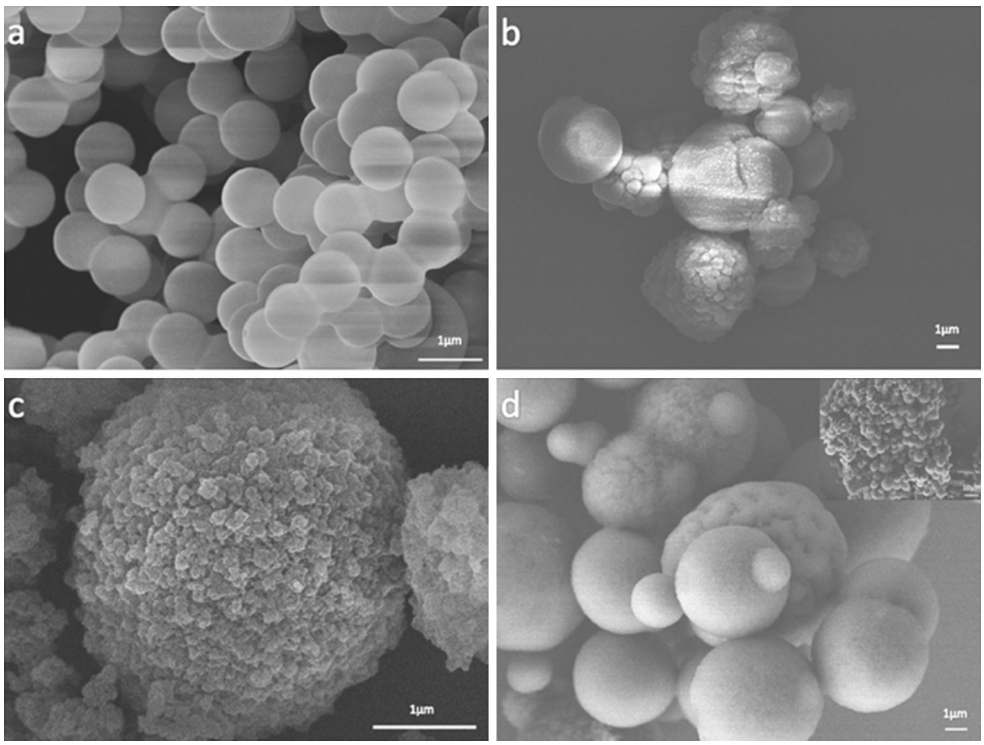

Fig. 2 SEM images of HTC (**a**), CCS-2 (**b**), CCS-3 (**c**) and CCS-4 (**d**)

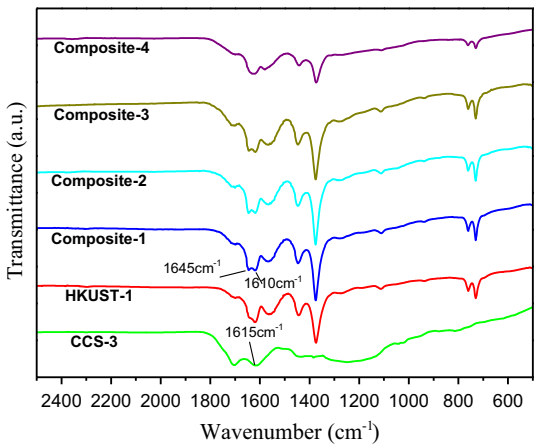

Fig. 3 FT-IR spectra of CCS-3, HKUST-1 and Composite-n

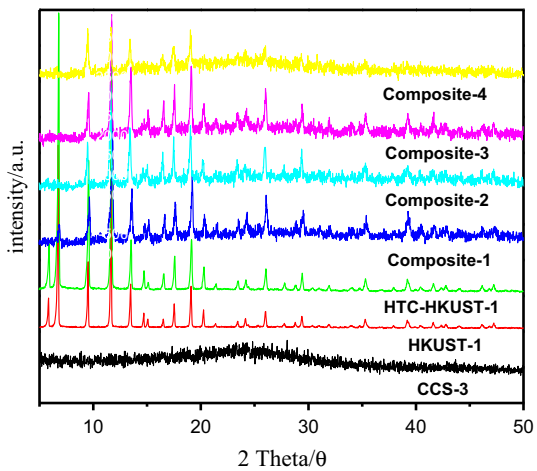

Fig. 4 XRD patterns of parent materials and Composite-n

blocks and the scattered CCSs increase (Fig. 5b–d), which offer sufficient surface space for the efficient growth of HKUST-1 due to the rich carboxyl groups. In contrast, the carboxyl groups on the HTC are lower than that of the CCSs, resulting in a weak interaction of the HKUST-1 with HTC. The SEM images of HTC-HKUST-1 shows the relatively smooth morphology, indicative of the low loading of HKUST-1 on HTC. This notable situation increases with increased HTC (Fig. 6). In Fig. 6 also shows the HKUST-1 blocks and scattered HTC are separated. This result is consistent with XRD of HTC-HKUST-1.

The EDS analysis of HTC-HKUST-1 shows the Cu contents of the HKUST-1 block and the scattered HTC are 28.15 and 6.41 wt% respectively (Fig. 7b, c). The Cu content of the HKUST-1 block is near to the theoretical value 29.20 wt% of the pure HKUST-1. The scattered HTC with low Cu content of 6.41 wt% is attributed to the HTC that has less carboxyl groups have weak interaction with HKUST-1. This result indicates most of the HKUST-1 growth by self accumulation. Also the Cu content of

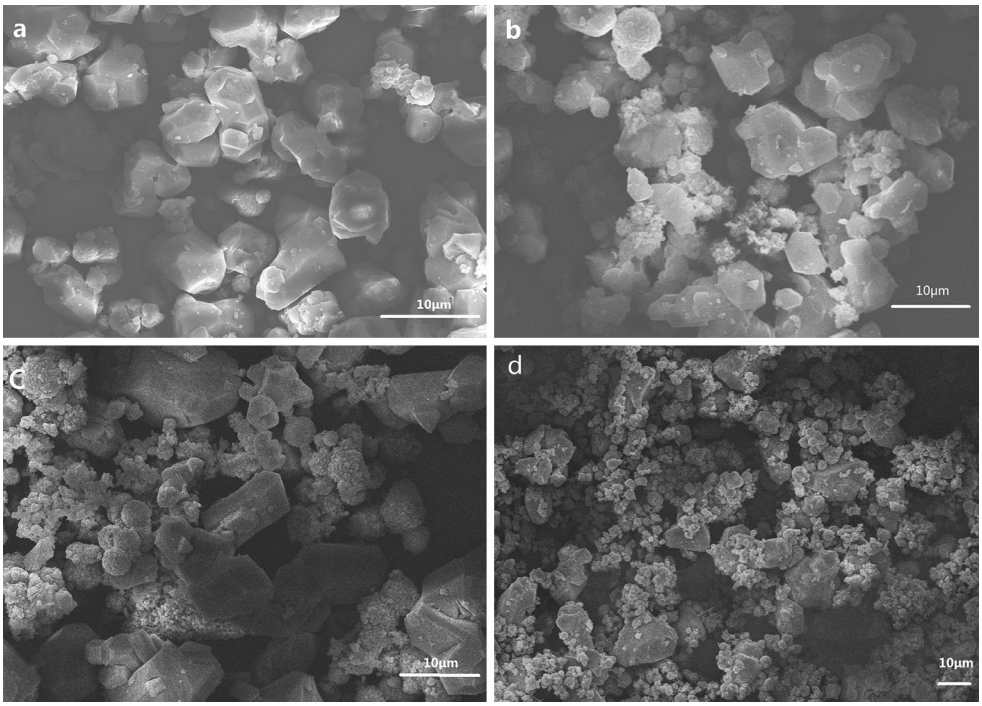

Fig. 5 SEM images of Composite-1 (**a**), Composite-2 (**b**), Composite-3 (**c**) and Composite-4 (**d**). The *inner figure* in **c** is the part of Composite-3

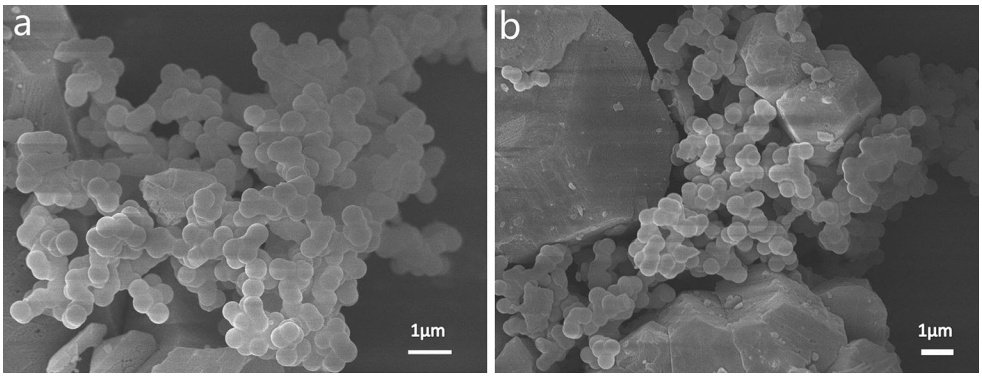

Fig. 6 SEM images of HTC-HKUST-1-A (**a**) and HTC-HKUST-1-B (**b**)

Composite-1 is 26.16 wt% by the EDS analysis (Fig. 7a), this result indicates there is a CCS core in the HKUST-1 shell resulting in the Cu content of Composite-1 decrease. We use the silicon wafer as basement, so the elemental peak of Si is clear in Fig. 7c. The average Cu content of Composite-1 analyzed by the ICP is 22.83 wt%, further calculated the amount of HKUST-1 is 78.48 wt%. To compare with the Cu content of Composite-1 analyzed by EDS (26.16 wt%), its normal the ICP result (22.83 wt%) is relatively lower, because the ICP result is an average value measured by a certain amount of Composite-1. The ICP result can be considered consistent with the result analyzed by EDS.

Figure 8 presents the TEM images of Composite-1 and Composite-3. It is observed that the edges of the composites have numerous porous channels, corresponding to the HKUST-1, and the black parts are attributed to the core part of CCSs [23]. This result proves that the MOFs are successfully covered on the CCSs surface.

The specific surface area of CCSs, HKUST-1, and the CCSs/HKUST-1 composites were further evaluated by nitrogen adsorption and desorption isotherm, and the pore size distribution calculated by the BJH method, as shown in Fig. 9. The hysteresis loops of HKUST-1(Fig. 9a) suggest the presence of mesopores, which might be those between the small crystals of MOF or composite particles [23]. It

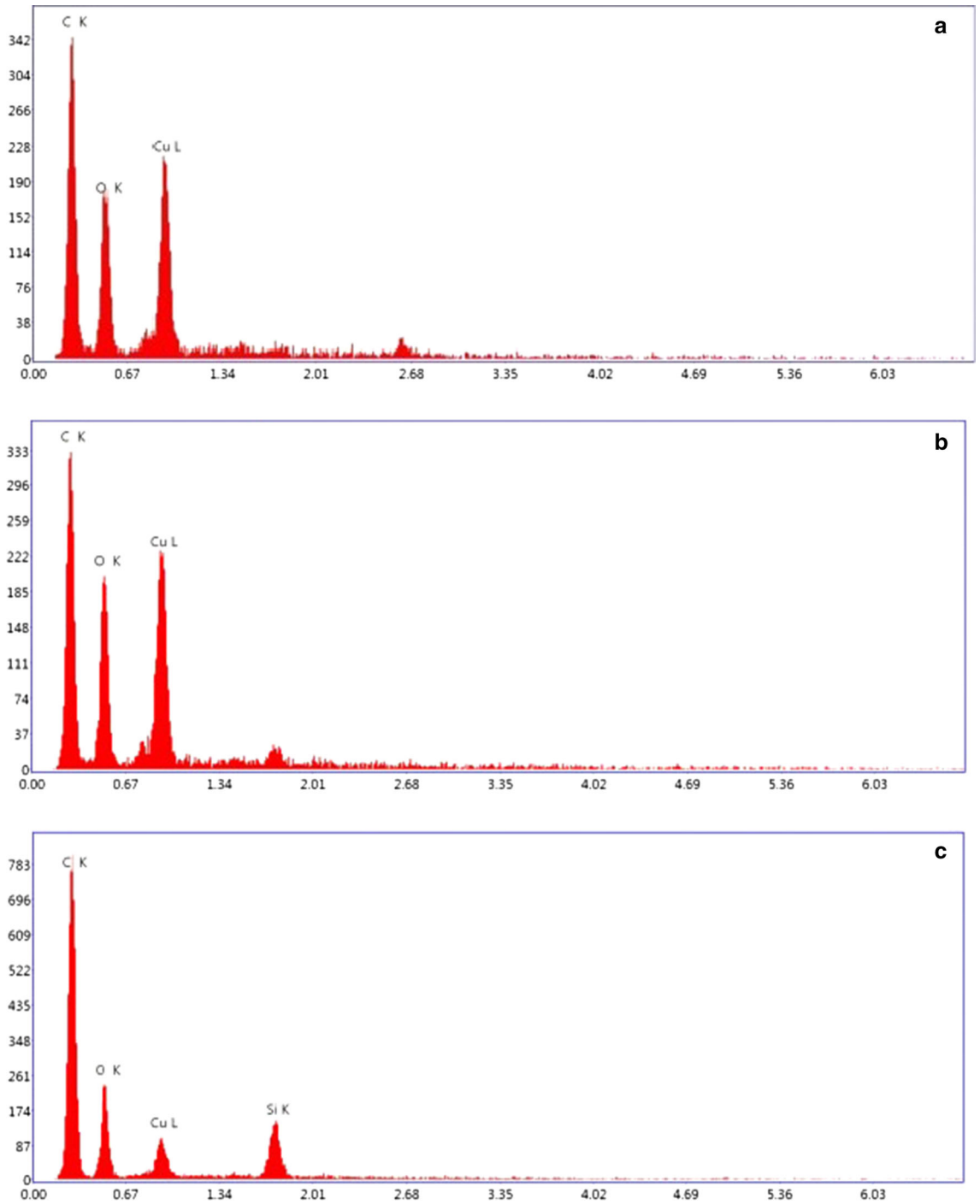

Fig. 7 EDS analysis of Composite-1 (**a**), HKUST-1 block in the HTC-HKUST-1 (**b**) and scattered HTC in the HTC-HKUST-1 (**c**)

can be seen that the specific surface area (S_{BET}) of Composite-1 with typical mesopore sharp peaks of 3.8 nm and 30 nm (Fig. 9b) is 495 m^2/g, which is higher than that of non-porous CCS-3 (31 m^2/g), and HKUST-1 (460 m^2/g), indicative of the successful introduction of the MOFs. The S_{BET} of Composite-1 is higher than that of pure HKUST-1. This result indicates that the synergy between CCS-3 and HKUST-1 increase Composite-1's porosity as well as the surface area. Further, when the CCS content in CCSs/HKUST-1 composites increases, the S_{BET} values slightly decrease from 355 m^2/g for Composite-2 to 343 m^2/g for Composite-3. Further, the optimized Composite-1 shows a higher micropore volume of 0.2 and larger ratio (V_{mic}/V_t) of micropore volume (V_{mic}) to total pore volume (V_t)

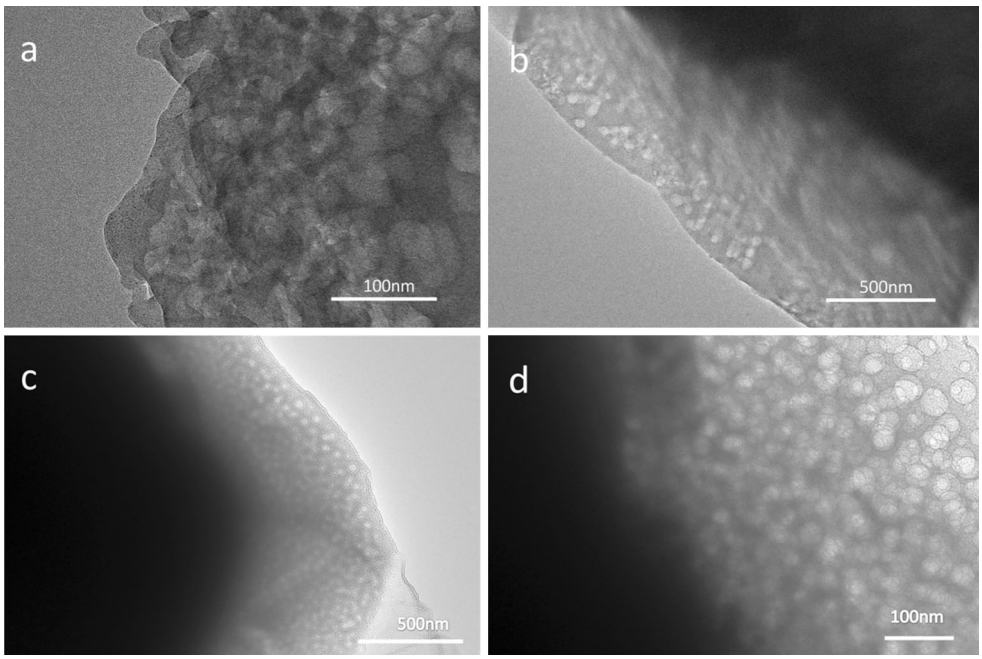

Fig. 8 TEM images of Composite-1 (**a**, **b**) and TEM micrographs of Composite-3 (**c**, **d**)

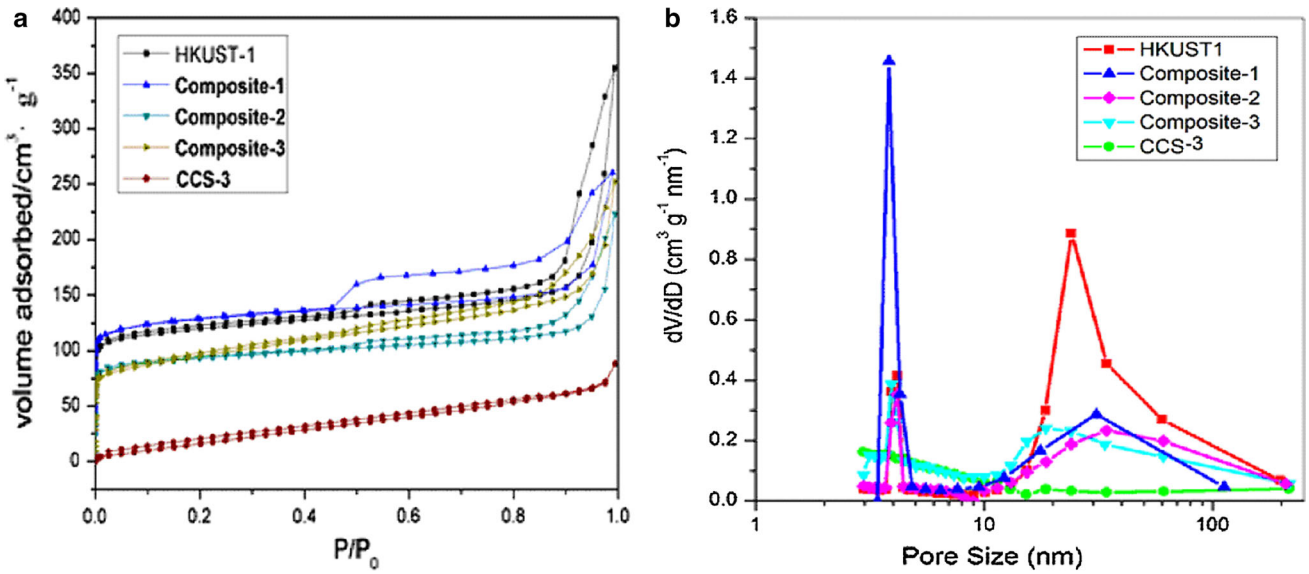

Fig. 9 Nitrogen adsorption, desorption isotherms (**a**) and pore size distribution (**b**) of CCSs, HKUST-1, and the CCSs/HKUST-1 composites, collected at 77 K and 1 atm pressure

Table 1 Comparison of the parameters of CCSs, HKUST-1, and the CCSs/HKUST-1 composites from N_2 sorption measurements

Sample	CCS content (%)	S_{BET} (m^2/g)	Pore volume, V_t (cc/g)	Micropore volume, V_{mic} (cc/g)	V_{mic}/V_t (%)
HKUST-1	0.0	460	0.55	0.15	26.9
Composite-1	9.9	495	0.40	0.20	49.3
Composite-2	14.1	355	0.35	0.12	33.3
Composite-3	21.5	343	0.39	0.08	20.8
CCS-3	100	31	0.14	0	0

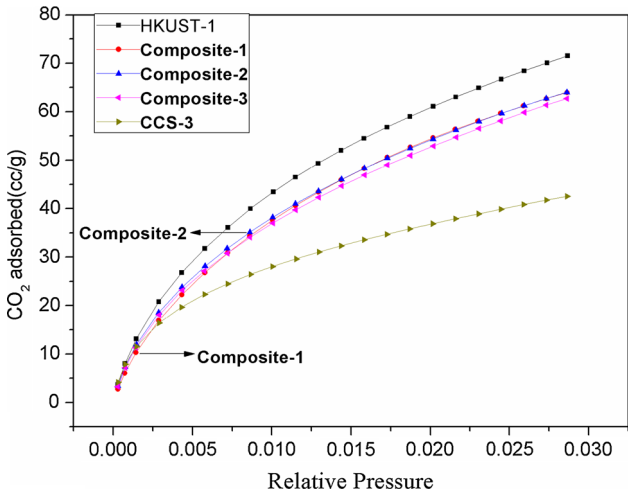

Fig. 10 CO_2 adsorption of the CCSs, HKUST-1, and the CCSs/HKUST-1 composites, collected at 273 K

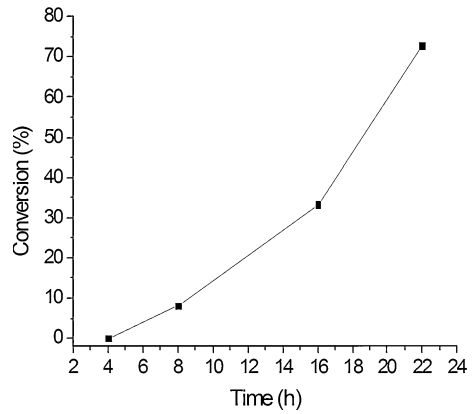

Fig. 11 Time conversion plot for the oxidation of benzyl alcohol to benzaldehyde catalyzed by Composite-1 and TEMPO

among the tested sample (Table 1). Similar results also are observed from the CO_2 adsorption measurement of the CCSs, HKUST-1, and the CCSs/HKUST-1 composites, collected under low relative pressure (<0.03), as presented in Fig. 10. It is disclosed that the CO_2 adsorption of composites is almost saturated at Composite-2, suggestive of the rich presence of micropores. Accordingly, the increase in CCSs does not significantly promote the increase of CO_2 adsorption.

Inspired by intrinsic high surface area, micro-/mesoporous structure, natural copper-containing MOF of $Cu_3(BTC)_2$ involved in electron transfer oxidation reactions of the CCSs/HKUST-1 composites, we are interested in studying the catalytic activity of such carbon/MOF spheres which directly transfers benzylic alcohols to benzaldehydes using molecular oxygen as the terminal oxidant promoted by $Cu_3(BTC)_2$ under mild conditions. To examine the potential, we further choose the optimized Composite-1 with high surface area and large pore volume as novel catalysts, in combination with TEMPO (2,2,6,6-tetramethyl-1-piperidinyloxy), for the catalytic oxidation of benzylic alcohol to the benzaldehyde. Figure 11 shows the time conversion plot for the oxidation of benzyl alcohol. It is revealed that the conversion of benzyl alcohol to benzaldehyde catalyzed by Composite-1 and TEMPO increase remarkably.

Very importantly, it is demonstrated that the final yield from benzylic alcohol to benzaldehyde using Composite-1 is up to 71.8 % after 22 h, which suggested the excellent catalytic properties of the CCSs/HKUST-1 composite. Notably, there is no trace of benzoic acid found in the reaction products. In sharp contrast, the yield from benzylic alcohol to benzaldehyde with pure HKUST-1 is only 33.3 % under the same experimental conditions. Composite-1 has better catalytic ability than pure HKUST-1. And to compare with pure HKUST-1, the Composite-1 has less HKUST-1 in the same weight. The core/shell structure of Composite-1 enhanced its catalytic ability. Comparison with other reported methods in the oxidation of benzylic alcohol, Composite-1 exhibited relatively well ability on conversion [24–27].

4 Conclusion

We demonstrated the designed synthesis of copper-based MOFs homogenously grown on the carboxyl-rich carbon-based spheres for efficient catalytic oxidation reaction of benzylic alcohol to benzaldehyde. It is disclosed that carboxyl-rich groups of the CCSs could substantially enhance the connection with the Cu ion in MOF, and benefit for the homogenous surface growth of HKUST-1 on the core of CCSs. The as-prepared composite exhibited a core/shell structure, high specific surface area, and microporous structures, and presented an impressive yield for oxidation reaction of benzylic alcohol to the benzaldehyde. The described strategy with carboxyl-rich nanocarbons coordinated with MOFs provides numerous opportunities to novel carbon-based MOFs hybrids for the certain applications in gas adsorption and catalytic reaction.

Acknowledgments The authors wish to thank the National Natural Science Foundation of China (Nos. 21171081/B0103 and 20971062/B010303), Natural Science Foundation of Liaoning Province (2013020085 and 201202093), Shenyang Science and Technology Plan Project (F13-289-1-00 and F14-231-1-10) for funding.

References

1. M.P. Suh, H.J. Park, T.K. Prasad, D.W. Lim, Chem. Rev. **112**, 782–835 (2012)
2. A.R. Millward, O.M. Yaghi, J. Am. Chem. Soc. **127**, 17998–17999 (2005)

3. J.R. Li, J. Sculley, H.C. Zhou, Chem. Rev. **112**, 869–932 (2012)
4. Z.Y. Wang, J.J. Wang, M.Y. Li, K.H. Sun, C.J. Liu, Sci. Rep. **4**, Article number: 5939 (2014)
5. M. Eddaoudi, H. Li, O.M. Yaghi, J. Am. Chem. Soc. **122**, 1391–1397 (2000)
6. D. Farrusseng, K. Schlichte, B. Spliethoff, A. Wingen, S. Kaskel, J.S. Bradley, F. Schuth, Angew. Chem. Int. Ed. **40**, 4204–4207 (2001)
7. H.K. Chae, D.Y. Siberio-Perez, J. Kim, Y.B. Go, M. Eddaoudi, A.J. Matzger, M. O'Keeffe, O.M. Yaghi, Nature **427**, 523–527 (2004)
8. H.J. Lee, W. Cho, M. Oh, Chem. Commun. **48**, 221–223 (2012)
9. S. Sorribas, B. Zornoza, C. Tellez, J. Coronas, Chem. Commun. **48**, 9388–9390 (2012)
10. A. Ahmed, M. Forster, R. Clowes, D. Bradshaw, P. Myers, H.F. Zhang, J. Mater. Chem. A **1**, 3276–3286 (2013)
11. M.G. Schwab, I. Senkovska, M. Rose, M. Koch, J. Pahnke, G. Jonschker, S. Kaskel, Adv. Eng. Mater. **10**, 1151–1155 (2008)
12. C. Petit, T. Bandosz, Adv. Mater. **21**, 4753–4757 (2009)
13. C. Petit, T. Bandosz, Adv. Funct. Mater. **20**, 111–118 (2010)
14. X. Sun, Y. Li, Angew. Chem. Int. Ed. **43**, 597–601 (2004)
15. S.S.-Y. Chui, S.M.-F. Lo, J.P.H. Charmant, A.G. Orpen, I.D. Williams, Science **283**, 1148–1150 (1999)
16. J.C. Liu, J.T. Culp, S. Natesakhawat, B.C. Bockrath, B. Zande, S.G. Sankar, G. Garberoglio, J.K. Johnson, J. Phys. Chem. C **111**, 9305–9313 (2007)
17. C. Petit, B. Mendoza, T. Bandosz, Langmuir **26**, 15302–15309 (2010)
18. H. Wang, L.J. Ma, K.C. Cao, J.X. Geng, J. Liu, Q. Song, X.D. Yang, S.J. Li, J. Hazard. Mater. **229–230**, 321–330 (2012)
19. R. Demir-Cakan, N. Baccile, M. Antonietti, M.M. Titirici, Chem. Mater. **21**, 484–490 (2009)
20. C. Petit, B. Mendoza, D. O'Donnell, T.J. Bandosz, Langmuir **27**, 10234–10242 (2011)
21. S. Vairam, S. Govindarajan, Thermochim. Acta **414**, 263–270 (2004)
22. C. Petit, B. Mendoza, T.J. Bandosz, Chem. Phys. Chem. **11**, 3678–3684 (2010)
23. C. Petit, J. Burress, T.J. Bandosz, Carbon **49**, 563–572 (2011)
24. H. Wang, C. Wang, H. Yan, H. Yi, J. Lu, J. Catal. **324**, 59–68 (2015)
25. B. Zahed, H. Hosseini-Monfared, Appl. Surf. Sci. **328**, 536–547 (2015)
26. I. Tamiolakis, I.N. Lykakis, G.S. Armatas, Catal. Today **250**, 180–186 (2015)
27. T. Harada, S. Ikeda, F. Hashimoto, T. Sakata, K. Ikeue, T. Torimoto, M. Matsumura, Langmuir **26**, 17720–17725 (2010)